NASA Contractor Report 165991

A FULL POTENTIAL INVERSE METHOD FOR WING DESIGN BASED ON A DENSITY LINEARIZATION SCHEME

Vijaya Shankar

ROCKWELL INTERNATIONAL SCIENCE CENTER
Thousand Oaks , CA 91360

Contract NAS1-16379
October 1982

NASA
National Aeronautics and
Space Administration

Langley Research Center
Hampton, Virginia 23665

A FULL POTENTIAL INVERSE METHOD BASED ON A DENSITY LINEARIZATION SCHEME FOR WING DESIGN

Vijaya Shankar

Rockwell International Science Center
Thousand Oaks, California 91360

SUMMARY

A mixed analysis-inverse procedure based on the full potential equation in conservation form has been developed to recontour a given base wing to produce a prescribed favorable pressure distribution. The method incorporates a novel density linearization scheme in applying the pressure boundary condition in terms of the velocity potential. The FLO30 finite volume analysis code has been modified to include the inverse option. The new surface shape information, associated with the modified pressure boundary condition, is calculated at a constant span station based on a mass flux integration. The inverse method is shown to recover the original shape when the analysis pressure is not altered. Inverse calculations for weakening of a strong shock system and for a laminar flow control (LFC) pressure distribution are presented. Two methods for trailing edge closure model are proposed for further study.

INTRODUCTION

Currently, the aircraft industry is in need of quick turnaround methods to develop energy efficient transonic configurations with optimal aerodynamic characteristics. Development of computational transonic methods over the last decade has significantly contributed towards fulfilling this need by aiding the design of efficient transonic airfoil sections and wing surfaces. Although computational models have been primarily developed to treat the direct problem of determining the load characteristics of a prescribed shape, the inverse problem associated with determining the required recontouring of a given wing to provide a preassigned favorable loading is becoming increasingly important to eliminate much of the cut-and-try approach to geometry definition.

Inverse methods based on the transonic small disturbance theory[1] in two[2] and three[3-4] dimensions and full potential models in two[5-6] and

three[7] dimensions have been developed with some restrictions or other. The small disturbance method[4] provides geometric versatility in designing fairly arbitrary geometries. However, the limitation of the method involves the breakdown of the theory for large flow deflections, especially near the leading edge. The existing full potential inverse method[7] that can handle the design of shocked flows is based on the nonconservative form of the full potential equation and uses the FL022 analysis code[8]. It is essential that the finite-difference approximation to the full potential equation be cast in conservation form to satisfy certain jump conditions[9] across the shock system. The nonconservative procedures[7,8] introduce mass sources at shock waves, and the strength of these sources depends on the local grid spacing, a non-physical consideration. Erroneous shock solutions could thus result in improper geometry definition while using inverse methods based on nonconservative formulation.

Other inverse methods such as the ones based on the "fictitious gas" approach[10-12] are oriented toward achieving shockless designs. Such a restriction may be too severe from the standpoint of aerodynamic efficiency, since some wave drag may be necessary for the production of a good lift-to-drag ratio. Of equal significance is the fact that a shockless wing could experience radical trim changes associated with sudden generation of large aerodynamic center shifts produced by shocks at slightly off-design conditions. In general, inverse methods provide a valuable alternative to optimization methods[13] which can provide shapes that optimize certain aerodynamic quantities but require excessive computer time for any realistic wing modification.

The present report deals with the development of an inverse method based on the fully conservative form of the full potential equation to address some of the limitations of the existing methods. The currently available FL030 finite volume full potential analysis code for wing-body combinations is modified to include the inverse option. The crux of the inverse problem is the incorporation of the prescribed pressure as a boundary condition on a surface yet to be determined as part of the solution procedure. A density linearization scheme is introduced in this report in applying the pressure boundary condition in terms of the velocity potential. Initially, the pressure boundary condition in terms of a Dirichlet problem is applied at the original shape location. After every n iterations ($n \sim 5$), the new shape information is

obtained at every span station using a mass flux integration procedure. Application of this inverse procedure to weaken the shock system of a typical transonic wing is illustrated. Another example of a wing design for laminar flow control pressure distribution is also demonstrated. The inverse method is reasonably inexpensive (35 to 45 minutes of CDC 7600 time for an analysis-inverse calculation) to use for wing modification requirements. The inverse program is also operational at the NASA-Langley Research Center using the CYBER 203 computing system.

At present, the currently developed inverse code is only a research tool and requires much more work to understand the constraints to be imposed on the specified pressure to achieve physically realistic looking shapes with closed trailing edges and also the relationship between the freestream Mach number and the specified pressure.

FORMULATION

The conservative form of the full potential equation in a general coordinate system ζ,η,ξ can be written as shown in Eq. (1) below. (This report uses $(x,y,z) \rightarrow (\zeta,\eta,\xi)$ as notation for the transformation. The use of $(x,y,z) \rightarrow (\xi,\eta,\zeta)$ is also common in the literature.)

$$\left(\rho \frac{U}{J}\right)_{\zeta} + \left(\rho \frac{V}{J}\right)_{\eta} + \left(\rho \frac{W}{J}\right)_{\xi} = 0 \ , \tag{1}$$

where U, V, and W are the contravariant velocity components, ρ is the density, and J is the Jacobian of the transformation that relates the general coordinates ζ,η,ξ to the Cartesian system x,y,z. Introducing the following notation for convenience

$$U_1 = U \ , \quad U_2 = V \ , \quad U_3 = W$$

$$x_1 = x \ , \quad x_2 = y \ , \quad x_3 = z$$

$$X_1 = \zeta \ , \quad X_2 = \eta \ , \quad X_3 = \xi$$

the contravariant velocities are given in terms of the velocity potential ϕ by

$$\left.\begin{aligned} U_i &= \sum_{j=1}^{3} a_{ij}\phi_{X_j} && i=1,2,3 \\ a_{ij} &= \sum_{k=1}^{3} \frac{\partial X_i}{\partial x_k}\frac{\partial X_j}{\partial x_k} && \begin{matrix} i=1,2,3 \\ j=1,2,3 \end{matrix} \end{aligned}\right\} . \tag{2}$$

The Jacobian of the transformation J is represented by

$$J = \frac{\partial(\zeta,\eta,\xi)}{\partial(x,y,z)} = \begin{bmatrix} \zeta_x & \zeta_y & \zeta_z \\ \eta_x & \eta_y & \eta_z \\ \xi_x & \xi_y & \xi_z \end{bmatrix} . \tag{3}$$

The density ρ is computed from the isentropic formula

$$\rho = \left[1 - \frac{\gamma-1}{2} M_\infty^2(q^2 - 1)\right]^{1/(1-\gamma)} \tag{4}$$

where the total velocity q is obtained from the relation

$$q^2 = \sum_{i=1}^{3} U_i \frac{\partial\phi}{\partial X_i} . \tag{5}$$

An analysis problem is one in which the Eq. (1) is solved to produce the flow field over a given geometry by imposing the usual surface tangency boundary condition $\phi_n = 0$ (n is normal to the body surface) on the exact surface location. If η is the coordinate leading out of the surface, then the surface tangency condition reduces to the simple form in terms of the contravariant velocity V

$$V = 0 \tag{6}$$

on the surface. After Eqs. (1) and (6) are solved together, the resulting pressure distribution over the surface is computed from

$$C_p = \frac{2}{\gamma M_\infty^2} (\rho^\gamma - 1) \ . \tag{7}$$

An inverse problem is one in which the Eq. (1) is solved subject to a prescribed pressure distribution (C_p specified) and the resulting body shape that satisfies the surface tangency condition Eq. (6) is sought.

Usually, for easy handling of the boundary condition, a body fitted coordinate system is chosen for ζ,η,ξ. Unlike the analysis boundary condition ($V = 0$), the incorporation of the inverse boundary condition in terms of a prescribed C_p (Eq. (7)) is considerably more difficult because the velocity potential ϕ appears nonlinearly through the ρ^γ term in Eq. (7). In order to aid in the application of the inverse boundary condition, first the density ρ appearing in the C_p relation is linearized as follows.

Density Linearization

From Eqs. (4) and (7), we can write

$$\left.\begin{aligned} \rho &= \left(\frac{C_p \gamma M_\infty^2}{2} + 1\right)^{1/\gamma} \\ &= \left[1 - \frac{\gamma-1}{2} M_\infty^2 \left(U\phi_\zeta + V\phi_\eta + W\phi_\xi - 1\right)\right]^{1/(\gamma-1)} \end{aligned}\right\} . \tag{8}$$

It can be seen from the above nonlinear relationship that from a given C_p distribution extracting the information in terms of the velocity potential ϕ would involve some type of a linearization. Denoting the current iteration cycle by (n+1) and the previous one by n, the variation in density due to variation in ϕ can be expressed as

$$\rho^{n+1} = \rho^n + \Delta\rho \tag{9}$$

where $\rho^n = \rho(\phi^n)$, $\Delta\rho = \rho(\phi^n + \Delta\phi) - \rho(\phi^n)$ and $\Delta\phi = (\phi^{n+1} - \phi^n)$. Rewriting Eq. (8) fully in terms of ϕ, $\rho(\phi)$ can be expressed as

$$[\rho(\phi)]^{(\gamma-1)} = \left\{1 - \frac{\gamma-1}{2} M_\infty^2 \left(\left[\sum_{i=1}^{3} \left(\sum_{j=1}^{3} a_{ij} \phi_{X_j} \right) \phi_{X_i} \right] - 1 \right) \right\} \quad . \tag{10}$$

Substituting $(\phi + \Delta\phi)$ in the place of ϕ in Eq. (10) and using binomial expansion, an expression for $\rho(\phi + \Delta\phi)$ can be written as

$$\rho^{n+1} = \rho(\phi + \Delta\phi) \doteq \rho^n - \left(\rho^n\right)^{2-\gamma} M_\infty^2 \left\{ U^n \frac{\partial}{\partial \zeta} + V^n \frac{\partial}{\partial \eta} + W^n \frac{\partial}{\partial \xi} \right\} \Delta\phi \quad . \tag{11}$$

The derivation of Eq. (11) is given in Appendix A.

While operating at the $(n+1)^{th}$ iteration cycle, all the quantities appearing at the n^{th} level are known and Eq. (11) can now be used to get an estimate for $\Delta\phi$ at the body surface for a given pressure distribution. Since we require $V = 0$ at the body, the given C_p can be expressed as

$$\rho^n - \left(\rho^n\right)^{2-\gamma} M_\infty^2 \underbrace{\left(U^n \frac{\partial}{\partial \zeta} + W^n \frac{\partial}{\partial \xi} \right)}_{\text{differential operator}} \left(\phi^{n+1} - \phi^n \right) = \left\{ \underbrace{C_p}_{\text{specified}} \frac{\gamma M_\infty^2}{2} + 1 \right\}^{1/\gamma} \quad . \tag{12}$$

In the inverse problem Eq. (12) will be discretized to get an estimate for $\Delta\phi = (\phi^{n+1} - \phi^n)$ which in turn will be used as a Dirichlet boundary condition while solving Eq. (1).

Implementation of Boundary Conditions

When Eq. (1) is discretized and written in terms of $\Delta\phi$ using Jameson's[15] pseudo-time concept, at any point (i,j,k) it will appear in tridiagonal form as

$$- TM(\Delta\phi)_{i,j-1,k} + T(\Delta\phi)_{i,j,k} - TP(\Delta\phi)_{i,j+1,k} = R \tag{13}$$

where TM, T, and TP are the coefficients of the tridiagonal system with built in artificial viscosity for handling mixed elliptic-hyperbolic flows and R is the finite-difference operator to be satisfied and is evaluated using

values of ϕ from the previous iteration and values of ϕ which have already been updated on the current iteration. Referring to Fig. 1, at any boundary point (● symbol) the evaluation of TM, T, TP, and R would require velocity potential information at the dummy points (□ symbol) that are introduced inside the body surface. Boundary conditions on the surface play a role in eliminating this dummy point information.

Analysis Problem

The analysis problem imposes V = 0 at all body points by simply reflecting all the various flux quantities across the surface. Referring to Fig. 1, this is done by setting

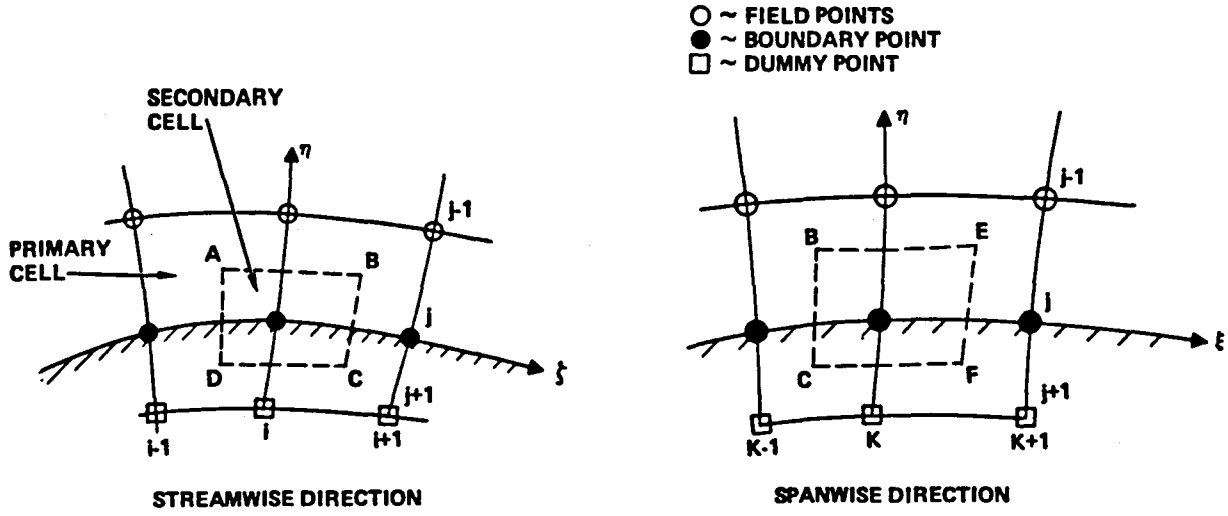

Fig. 1. Boundary cell distribution

$$\left.\begin{aligned}\left(\rho\,\frac{V}{J}\right)_{D,C,F} &= -\left(\rho\,\frac{V}{J}\right)_{A,B,E}\\ \left(\rho\,\frac{U}{J}\right)_{D,C,F} &= \left(\rho\,\frac{U}{J}\right)_{A,B,E}\\ \left(\rho\,\frac{W}{J}\right)_{D,C,F} &= \left(\rho\,\frac{W}{J}\right)_{A,B,E}\end{aligned}\right\}. \qquad (14)$$

Equation (14) would automatically set $V^n = 0$ while forming R^n, TM, T, and TP, but doesn't rigorously satisfy $V^{n+1} = 0$ which is the actual boundary condition to be imposed. This can probably be achieved if $(\Delta\phi)_{i,j+1,k}$ corresponding to the dummy point can be replaced in terms of information on the surface and above the surface appropriately. In the present method $(\Delta\phi)_{i,j+1,k}$ is simply set to zero while solving for the body point.

Inverse Problem

Referring to Fig. 2, when Eq. (13) is written at one point above the body surface (point A at i,j-1,k), it involves $(\Delta\phi)_{i,j,k}$ appearing at the body point. In the inverse problem, the value for $(\Delta\phi)_{i,j,k}$ at the body point is first computed from the prescribed pressure distribution using the density linearization procedure given by Eq. (12), in the following way. Referring to Fig. 3, the pressure coefficient is prescribed at the center (* symbol) of

SC82-18227

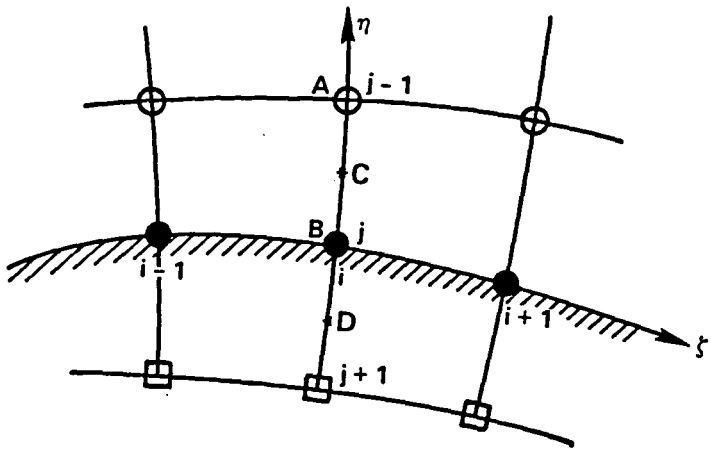

Fig. 2.
Grid point notation for the inverse procedure

each primary cell face coinciding with the body surface. First consider the lower surface where along the direction of sweep the index i increases. The discretized form of Eq. (12) can be written as (at point P in Fig. 3)

$$\rho_P^n - \left(\rho_P^n\right)^{2-\gamma} \frac{M_\infty^2}{2} \left\{ \frac{U_P^n}{\Delta\xi}\left(\Delta\phi_S - \Delta\phi_R + \Delta\phi_T - \Delta\phi_Q\right) + \frac{W_P^n}{\Delta\zeta}\left(\Delta\phi_S - \Delta\phi_T + \Delta\phi_R - \Delta\phi_Q\right) \right\}$$

$$= \left\{ \left(C_p\right)_P \frac{\gamma M_\infty^2}{2} + 1 \right\}^{1/\gamma} . \qquad (15)$$

Since the direction of sweep is along increasing k-index in the span direction and increasing i-index in the streamwise direction at the lower surface, the quantities $(\Delta\phi)_R$, $(\Delta\phi)_Q$, and $(\Delta\phi)_T$ are known and the unknown to be computed from Eq. (15) is $(\Delta\phi)_S = (\Delta\phi)_{i,j,k}$. This is required while solving Eq. (13) at point A in Fig. 2. On the upper surface where the i-index is decreasing along the direction of sweep, C_p prescribed at $(i+\frac{1}{2},k-\frac{1}{2})$ is used to compute $(\Delta\phi)_{i,j,k}$. For example (in Fig. 3) the pressure coefficient at point N and $(\Delta\phi)_H$, $(\Delta\phi)_G$, and $(\Delta\phi)_L$ will be used to compute $(\Delta\phi)_M = (\Delta\phi)_{i,j,k}$ in a manner similar to the Eq. (15) for the lower surface. While solving Eq. (13) at point A in Fig. 2, the quantity $TP(\Delta\phi)_{i,j,k}$ is known from the above procedure and is lumped into the right-hand side residual term and Eq. (1) is solved only up to one point above the body surface. Thus, the inverse problem uses a Dirichlet boundary condition.

New Shape Information

Initially, the pressure boundary condition is applied at the original shape location. After every n inverse relaxation cycles ($n \sim 5$ to 10), the new shape information is obtained by using a mass flux integration procedure as follows.

Referring to Fig. 2, point B is on the old surface where the specified pressure condition, in terms of $(\Delta\phi)_B$, was imposed as a Dirichlet boundary condition. After a vertical line relaxation is completed, the finite differenced form of Eq. (1) given by Eq. (13) is solved at point B, using $(\Delta\phi)_B$ and $(\Delta\phi)_A$ now available. The dummy point value of $\Delta\phi$ ($\Delta\phi_{j+1}$ in Eq. (13)) is set to zero, just as in the analysis problem. The right hand side R in Eq. (13) at point B can be represented as $R = R\left\{\left(\rho \frac{V}{J}\right)_C, \left(\rho \frac{V}{J}\right)_D, \cdots\right\}$. In an analysis calculation $\left(\rho \frac{V}{J}\right)_D$ is set equal to $-\left(\rho \frac{V}{J}\right)_C$. But, for an inverse problem, where the new shape information is sought, the flux value $\left(\rho \frac{V}{J}\right)_D$ will not be equal to $-\left(\rho \frac{V}{J}\right)_C$. By accepting the value for $\left(\rho \frac{V}{J}\right)_C$ as it exists at point C, solution to Eq. (13) at point B will yield a value for the flux $\left(\rho \frac{V}{J}\right)_D$. The modified flux information at the old surface point B is taken to be $\left(\rho \frac{V}{J}\right)_B = \frac{1}{2}\left\{\left(\rho \frac{V}{J}\right)_C + \left(\rho \frac{V}{J}\right)_D\right\}$. Again, this will not be zero for an inverse calculation. Once the modified flux information is known at the old surface points, the new shape information can be obtained. Let the dashed line in Fig. 4 represent the modified new shape. The surface transpiration at i-1 grid point is denoted by $(d\eta)_{i-1}$, and at point B by $(d\eta)_i$. Balancing the mass flux between the old shape (solid line) and the new shape (dashed line), the following relationship is obtained (neglecting the effect of the spanwise variation)

$$\left\{\left(\rho \frac{U}{J}\right)_i (d\eta)_i - \left(\rho \frac{U}{J}\right)_{i-1} (d\eta)_{i-1}\right\} - \frac{\left\{\left(\rho \frac{V}{J}\right)_i + \left(\rho \frac{V}{J}\right)_{i-1}\right\}}{2} \left(\zeta_i - \zeta_{i-1}\right) = 0 \quad . \quad (16)$$

Equation (16) assumes that V is zero along the dashed line (boundary condition for a solid surface). The only unknown in Eq. (16) is $(d\eta)_i$. Usually, the nose shape is prescribed, and the starting value of $(d\eta)_{i-1}$ is zero at the point of transition from analysis to inverse. Once $(d\eta)_i$ is known, the new values of x and y at point $\bar{B}$ are computed as follows:

$$\left.\begin{aligned} x_{\bar{B}} &= x_B + \left(x_\eta\right)_B (d\eta)_i \\ y_{\bar{B}} &= y_B + \left(y_\eta\right)_B (d\eta)_i \end{aligned}\right\} \qquad (17)$$

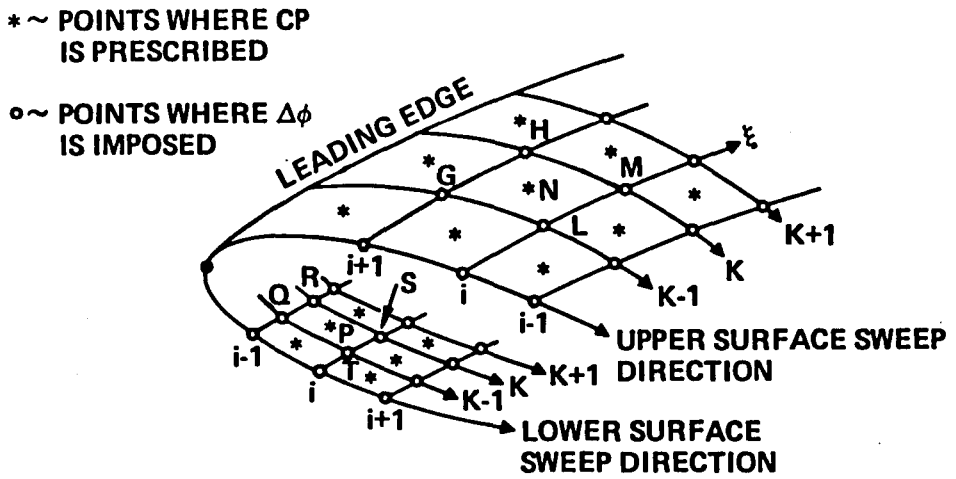

Fig. 3. Prescription of C_p at midpoints on the upper and lower surface

SC82-18224

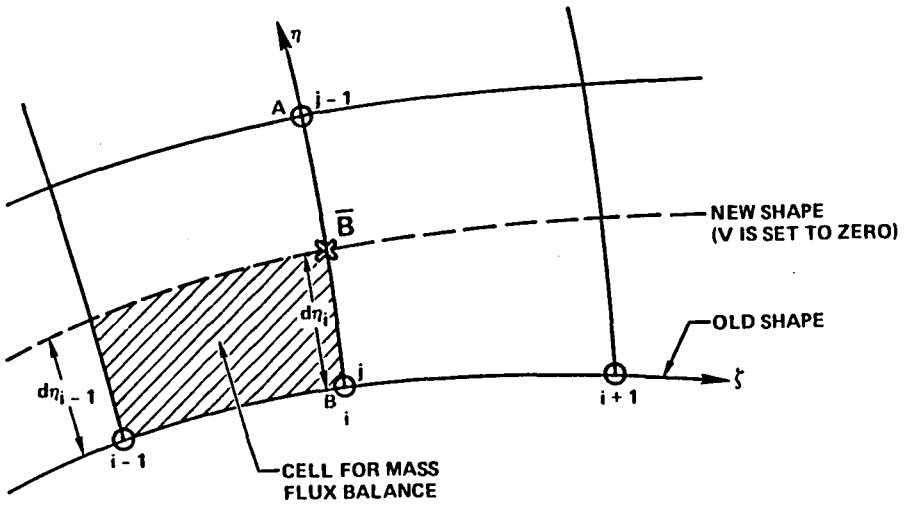

Fig. 4. Construction of new shape

where $(x_\eta)_B$ and $(y_\eta)_B$ are obtained by three-point one-sided differentiation.

RESULTS

The finite volume FL030 code[15,16] is an analysis code based on the full potential equation in conservation form and has the capability to handle wing-body combinations. The inverse procedure presented in this paper is also based on the full potential equation in conservation form and the FL030 analysis program is found to be a good choice to incorporate the inverse logic. One advantage of using the FL030 program is that it requires only a local description of the coordinate mapping to a body-fitted system and essentially decouples the solution process from the generation of the grid network. As a result, during the inverse calculation as shape changes take place, this method requires grid adjustments only to local cells adjacent to the wing rather than having to change the entire grid distribution at the end of each relaxation cycle.

To test the inverse concept, first an analysis calculation was performed using a typical transonic wing geometry definition as shown in Fig. 5, at $M_\infty = 0.86$ and freestream angle of attack of 4.68°. After a sequence of crude-medium-fine grid calculations (approximately 30 minutes of computer time on the CDC 7600 machine using a $161 \times 27 \times 35$ fine grid), the analysis calculation was reasonably converged. The resulting pressure distributions on the upper surface at discrete span stations are shown in Fig. 5. The presence of a shock system is evident and the strength of the shock gradually increases from the wing root reaching a peak strength around 85% span. As a verification for the correctness of the inverse procedure, the analysis pressure of Fig. 5 is kept unaltered and specified as input pressure for the inverse calculation. After 20 inverse cycles, the resulting shape information is provided in a tabular form from the computer output in Table 1. It has eight columns. Explanations for Columns (1) to (8) are given below.

Column (1): Value of x/c at that span station.

Column (2): Value of x of the surface grid point.

Column (3): Value of Y of the grid point on the original shape.

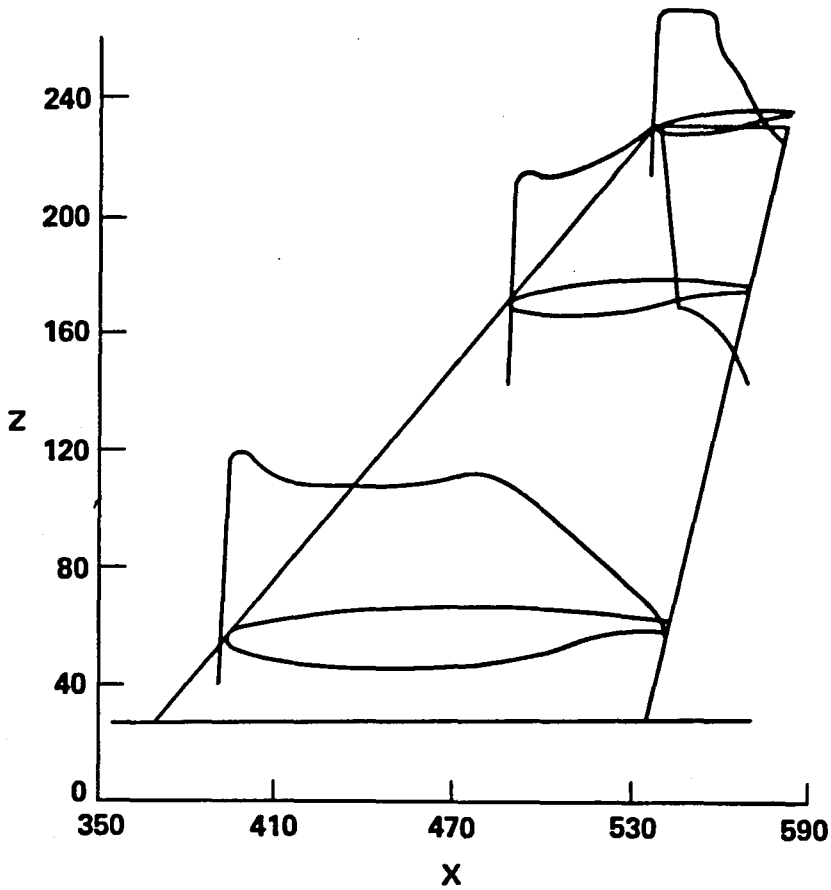

Fig. 5. Typical transonic wing showing presence of a shock system at $M_\infty = 0.86$, $\alpha = 4.86°$

Column (4): Value of z of the surface grid point.

Column (5): C_p at node point on the surface (i,j,k).

Column (6): C_p at half node point (prescribed).

Column (7): Value of Y of the grid point on the new shape.

Column (8): Index i in the ζ direction.

In Table 1, the C_p in column (6) is the same as the analysis calculation of Fig. 5. The resulting shape information in column (7) very closely duplicates the original shape given in column (3).

Table 1. Recovery of original shape for unaltered analysis pressure specification, $M_\infty = 0.86$, $\alpha = 4.86°$. (Explanations of columns (1) through (8) are on pages 12 and 13.)

SECTION CHARACTERISTICS

PCT SEMISPAN .5614 (1)	(2)	CL .3348 (3)	(4)	CD .0036 (5)	(6)	CM -.1685 (7)	(8)
1.000	559.301	118.567	127.750	.178	.185	118.620	29
.967	555.793	118.778	127.711	.141	.167	118.831	30
.934	552.338	119.139	127.696	.046	.109	119.191	31
.902	548.918	119.491	127.660	-.073	-.030	119.543	32
.870	545.538	119.736	127.647	-.128	-.132	119.788	33
.839	542.196	119.917	127.641	-.136	-.141	119.969	34
.808	538.894	120.095	127.635	-.145	-.145	120.148	35
.777	535.632	120.251	127.631	-.158	-.159	120.304	36
.747	532.410	120.406	127.620	-.188	-.169	120.459	37
.717	529.229	120.553	127.601	-.290	-.209	120.607	38
.687	526.094	120.661	127.587	-.458	-.389	120.715	39
.658	523.004	120.759	127.575	-.568	-.522	120.814	40
.630	519.961	120.836	127.565	-.617	-.594	120.890	41
.601	516.967	120.881	127.560	-.630	-.618	120.936	42
.574	514.024	120.898	127.559	-.622	-.619	120.952	43
.546	511.134	120.876	127.563	-.608	-.605	120.930	44
.520	508.297	120.835	127.570	-.599	-.591	120.888	45
.493	505.514	120.776	127.579	-.586	-.586	120.829	46
.468	502.788	120.687	127.590	-.570	-.569	120.739	47
.443	500.119	120.571	127.603	-.553	-.549	120.622	48
.418	497.509	120.445	127.617	-.543	-.539	120.495	49
.394	494.960	120.301	127.634	-.536	-.530	120.350	50
.371	492.472	120.146	127.652	-.535	-.525	120.194	51
.348	490.049	119.979	127.671	-.538	-.526	120.026	52
.326	487.690	119.802	127.692	-.543	-.532	119.849	53
.304	485.398	119.612	127.714	-.544	-.538	119.656	54
.283	483.174	119.407	127.736	-.539	-.535	119.450	55
.263	481.020	119.186	127.764	-.537	-.528	119.228	56
.243	478.936	118.965	127.789	-.539	-.532	119.005	57
.224	476.927	118.723	127.817	-.535	-.534	118.762	58
.206	474.993	118.479	127.847	-.530	-.525	118.516	59
.189	473.135	118.227	127.876	-.525	-.522	118.263	60
.172	471.354	117.963	127.907	-.515	-.515	117.996	61
.156	469.651	117.694	127.937	-.503	-.503	117.726	62
.140	468.027	117.418	127.968	-.491	-.490	117.448	63
.126	466.483	117.143	127.998	-.487	-.482	117.171	64
.112	465.019	116.869	128.026	-.493	-.483	116.895	65
.099	463.635	116.595	128.054	-.504	-.491	116.622	66
.087	462.335	116.324	128.082	-.509	-.503	116.346	67
.075	461.119	116.044	128.109	-.507	-.502	116.064	68
.065	459.985	115.767	128.136	-.507	-.504	115.785	69

Table 1 (Continued)

.046	457.972	115.212	128.187	-.515	-.510	115.226	71
.038	457.093	114.931	128.212	-.523	-.514	114.942	72
.030	456.295	114.658	128.235	-.539	-.529	114.667	73
.023	455.581	114.377	128.259	-.533	-.546	114.384	74
.017	454.953	114.084	128.283	-.510	-.517	114.088	75
.012	454.399	113.793	128.306	-.482	-.503	113.794	76
.008	453.933	113.476	128.330	-.395	-.459	113.476	77
.004	453.548	113.139	128.355	-.235	-.331	113.139	78
.002	453.277	112.761	128.382	.063	-.131	112.761	79
.000	453.142	112.352	128.410	.264	.147	112.352	80
0.	453.109	111.944	128.437	.457	.378	111.944	81
.001	453.171	111.542	128.462	.568	.526	111.542	82
.002	453.325	111.148	128.485	.598	.594	111.148	83
.004	453.576	110.766	128.507	.553	.586	110.766	84
.008	453.922	110.397	128.526	.454	.515	110.397	85
.012	454.373	110.055	128.544	.340	.401	110.061	86
.017	454.913	109.733	128.559	.230	.292	109.750	87
.023	455.545	109.431	128.573	.127	.185	109.456	88
.030	456.276	109.170	128.585	.045	.089	109.198	89
.038	457.095	108.934	128.595	-.012	.021	108.964	90
.046	458.000	108.723	128.604	-.050	-.027	108.756	91
.055	458.990	108.531	128.611	-.079	-.057	108.566	92
.065	460.062	108.349	128.618	-.108	-.085	108.387	93
.076	461.219	108.187	128.624	-.130	-.115	108.228	94
.088	462.458	108.041	128.630	-.144	-.131	108.084	95
.100	463.779	107.907	128.634	-.159	-.143	107.953	96
.114	465.180	107.780	128.639	-.179	-.161	107.828	97
.128	466.662	107.668	128.642	-.197	-.182	107.718	98
.142	468.224	107.574	128.646	-.210	-.197	107.627	99
.156	469.864	107.492	128.648	-.223	-.205	107.547	100
.174	471.582	107.426	128.650	-.235	-.222	107.483	101
.191	473.376	107.373	128.652	-.247	-.233	107.432	102
.208	475.245	107.336	128.653	-.256	-.246	107.396	103
.227	477.188	107.317	128.654	-.268	-.252	107.379	104
.246	479.201	107.299	128.656	-.289	-.270	107.362	105
.265	481.286	107.310	128.657	-.305	-.292	107.373	106
.286	483.441	107.338	128.658	-.317	-.305	107.402	107
.307	485.665	107.381	128.658	-.328	-.319	107.446	108
.328	487.957	107.446	128.657	-.341	-.329	107.511	109
.350	490.314	107.528	128.657	-.357	-.346	107.594	110
.373	492.736	107.634	128.655	-.371	-.364	107.700	111
.397	495.221	107.765	128.652	-.384	-.378	107.831	112
.421	497.767	107.922	128.649	-.394	-.394	107.988	113
.445	500.373	108.115	128.644	-.399	-.403	108.182	114
.470	503.039	108.342	128.637	-.398	-.407	108.409	115
.496	505.761	108.611	128.627	-.383	-.407	108.679	116
.522	508.540	108.932	128.613	-.350	-.376	109.002	117
.549	511.372	109.304	128.596	-.308	-.337	109.374	118
.576	514.257	109.737	128.576	-.254	-.289	109.809	119
.603	517.192	110.238	128.550	-.185	-.225	110.312	120

Table 1 (Concluded)

.660	523.205	111.410	128.484	-.031	-.073	111.488	122
.689	526.281	112.060	128.442	.045	.006	112.140	123
.718	529.400	112.721	128.397	.113	.078	112.803	124
.748	532.563	113.384	128.348	.173	.142	113.468	125
.778	535.767	114.030	128.289	.227	.199	114.116	126
.809	539.013	114.658	128.221	.276	.252	114.738	127
.840	542.298	115.224	128.154	.323	.301	115.314	128
.871	545.624	115.719	128.091	.362	.343	115.811	129
.903	548.989	116.130	128.033	.391	.379	116.223	130
.935	552.393	116.396	127.989	.401	.403	116.490	131
.967	555.836	116.477	127.963	.365	.400	116.570	132
1.000	559.301	116.317	127.932	.269	.329	116.406	133

Next, the analysis pressure distribution with a strong shock system was modified on the upper surface from 50% to 95% span in such a way that the shock strength is considerably reduced. The modified pressures were then used as an input to the inverse code and the inverse calculations were started from the converged analysis results. After 50 fine grid cycle inverse calculations (15 minutes of CPU time), the residual and the maximum change in the velocity potential were of the same order as the converged analysis calculations. A sample output of this inverse calculation at 70% span station is shown in tabular form in Table 2. The shape differences between the original shape and the modified shape can be seen by comparing column (3) and column (7). Figure 6 shows the same results in graphical form. The openness of the trailing edge for the modified shape is much smaller than the original shape.

One other design problem reported here is a laminar flow control wing design. The objective here is to start with the base wing geometry shown in Figs. 7 and 8, and then modify the airfoil sections in the test strip shown in Fig. 7 to produce a laminar flow control pressure distribution shown in Fig. 9 at the midspan region. This is a very difficult design problem because the prescribed pressure is considerably different from the one produced by the base wing geometry. Like the previous example, the inverse calculation with the specified LFC pressure at 50% span was started from the analysis calculation. After 50 design cycles (the modified shape was computed at the end of every 5 cycles and updated), the resulting modified shapes at two different span stations to provide the LFC pressure of Fig. 9 at midspan, are shown in

Table 2. Computer output at 70% span indicating the old and new shape for an inverse calculation to weaken the shock strength, $M_\infty = 0.86$, $\alpha = 4.86°$

SECTION CHARACTERISTICS

PCT SEMISPAN		CL		CD	CM		
.6932		.3414		-.0034	-.1724		
(1)	(2)	(3)	(4)	(5)	(6)	(7)	(8)
1.000	566.782	116.347	157.993	.190	.200	114.951	29
.967	563.866	116.449	157.963	.168	.132	114.985	30
.934	560.993	116.653	157.923	.101	.145	115.169	31
.902	558.148	116.868	157.881	.007	.040	115.327	32
.870	555.338	117.030	157.865	-.081	-.054	115.368	33
.839	552.563	117.159	157.865	-.149	-.130	115.381	34
.808	549.820	117.292	157.864	-.203	-.178	115.465	35
.777	547.111	117.405	157.866	-.263	-.230	115.591	36
.747	544.436	117.515	157.867	-.323	-.274	115.814	37
.717	541.797	117.620	157.869	-.390	-.337	116.139	38
.687	539.195	117.691	157.873	-.432	-.424	116.533	39
.658	536.632	117.752	157.879	-.444	-.447	116.996	40
.629	534.107	117.795	157.886	-.493	-.464	117.396	41
.601	531.622	117.805	157.886	-.572	-.542	117.613	42
.573	529.179	117.790	157.889	-.619	-.609	117.700	43
.546	526.779	117.742	157.894	-.626	-.625	117.704	44
.520	524.424	117.677	157.901	-.627	-.620	117.664	45
.493	522.115	117.596	157.909	-.624	-.624	117.586	46
.468	519.854	117.483	157.921	-.609	-.612	117.466	47
.443	517.640	117.359	157.933	-.595	-.593	117.331	48
.418	515.477	117.221	157.946	-.587	-.586	117.180	49
.394	513.364	117.068	157.961	-.581	-.577	117.014	50
.371	511.302	116.907	157.976	-.578	-.573	116.840	51
.348	509.294	116.737	157.992	-.579	-.572	116.657	52
.326	507.340	116.559	158.008	-.584	-.576	116.464	53
.304	505.441	116.372	158.025	-.582	-.580	116.265	54
.283	503.595	116.178	158.042	-.572	-.573	116.065	55
.263	501.813	115.967	158.058	-.568	-.564	115.846	56
.243	500.086	115.758	158.074	-.572	-.566	115.628	57
.225	498.419	115.540	158.090	-.568	-.569	115.404	58
.206	496.814	115.312	158.107	-.558	-.556	115.174	59
.189	495.270	115.084	158.124	-.551	-.551	114.947	60
.172	493.791	114.848	158.141	-.541	-.544	114.713	61
.156	492.376	114.610	158.158	-.529	-.531	114.480	62
.141	491.026	114.367	158.175	-.520	-.518	114.245	63
.126	489.742	114.127	158.192	-.517	-.513	114.018	64
.112	488.523	113.889	158.206	-.520	-.510	113.798	65
.099	487.372	113.655	158.223	-.531	-.518	113.583	66
.087	486.289	113.417	158.239	-.535	-.532	113.366	67
.075	485.276	113.175	158.254	-.528	-.527	113.146	68
.065	484.331	112.935	158.269	-.520	-.523	112.931	69

Table 2 (Continued)

.055	483.458	112.691	158.284	-.513	-.513	112.710	70
.046	482.652	112.452	158.299	-.507	-.511	112.489	71
.037	481.918	112.206	158.313	-.500	-.503	112.254	72
.030	481.250	111.964	158.327	-.503	-.505	112.014	73
.023	480.654	111.714	158.341	-.516	-.511	111.749	74
.017	480.129	111.453	158.356	-.503	-.527	111.468	75
.012	479.669	111.188	158.370	-.442	-.488	111.192	76
.007	479.282	110.904	158.385	-.324	-.413	110.904	77
.004	478.968	110.601	158.400	-.144	-.260	110.601	78
.001	478.753	110.266	158.417	.091	-.053	110.266	79
.000	478.648	109.914	158.434	.324	.204	109.914	80
0.	478.625	109.568	158.449	.489	.409	109.565	81
.001	478.681	109.229	158.464	.577	.539	109.229	82
.002	478.814	108.899	158.478	.583	.591	108.899	83
.005	479.030	108.583	158.491	.515	.562	108.583	84
.008	479.326	108.284	158.502	.395	.469	108.284	85
.012	479.712	108.018	158.512	.266	.342	108.019	86
.017	480.165	107.763	158.522	.148	.218	107.774	87
.023	480.694	107.529	158.530	.049	.110	107.559	88
.030	481.303	107.329	158.537	-.023	.022	107.371	89
.038	481.984	107.151	158.543	-.072	-.039	107.203	90
.047	482.736	106.992	158.548	-.104	-.079	107.055	91
.056	483.557	106.848	158.553	-.131	-.106	106.921	92
.066	484.446	106.714	158.557	-.157	-.134	106.795	93
.077	485.405	106.596	158.561	-.176	-.161	106.685	94
.089	486.433	106.491	158.565	-.187	-.175	106.588	95
.101	487.528	106.396	158.568	-.201	-.184	106.500	96
.114	488.689	106.308	158.571	-.220	-.202	106.419	97
.128	489.918	106.232	158.574	-.237	-.224	106.349	98
.143	491.214	106.172	158.576	-.248	-.237	106.295	99
.158	492.574	106.122	158.578	-.259	-.248	106.251	100
.174	493.999	106.086	158.580	-.269	-.259	106.220	101
.191	495.487	106.061	158.582	-.280	-.269	106.201	102
.209	497.037	106.049	158.583	-.287	-.280	106.193	103
.227	498.649	106.055	158.584	-.296	-.284	106.202	104
.246	500.321	106.060	158.585	-.314	-.300	106.212	105
.266	502.052	106.090	158.585	-.323	-.321	106.245	106
.286	503.842	106.144	158.585	-.326	-.321	106.302	107
.307	505.689	106.194	158.584	-.336	-.329	106.355	108
.329	507.592	106.271	158.581	-.346	-.342	106.435	109
.351	509.549	106.364	158.578	-.352	-.349	106.530	110
.374	511.560	106.476	158.575	-.360	-.357	106.645	111
.397	513.623	106.611	158.571	-.368	-.365	106.781	112
.421	515.736	106.767	158.566	-.373	-.374	106.939	113
.446	517.899	106.955	158.560	-.373	-.376	107.129	114
.471	520.111	107.168	158.553	-.372	-.376	107.342	115
.496	522.369	107.421	158.544	-.359	-.375	107.595	116
.522	524.674	107.721	158.534	-.329	-.350	107.894	117
.549	527.023	108.060	158.521	-.288	-.314	108.231	118
.576	529.415	108.452	158.506	-.236	-.269	108.620	119

Table 2 (Concluded)

.632	534.322	109.405	158.465	-.095	-.135	109.566	121
.660	536.834	109.941	158.433	-.029	-.059	110.098	122
.689	539.384	110.515	158.397	.053	.016	110.668	123
.719	541.970	111.099	158.358	.119	.067	111.248	124
.748	544.591	111.686	158.316	.178	.149	111.830	125
.778	547.248	112.259	158.271	.231	.205	112.400	126
.809	549.939	112.813	158.225	.280	.256	112.951	127
.840	552.663	113.327	158.180	.323	.304	113.464	128
.871	555.421	113.777	158.136	.359	.342	113.914	129
.903	558.215	114.162	158.110	.387	.376	114.301	130
.935	561.044	114.433	158.108	.397	.399	114.577	131
.967	563.906	114.555	158.119	.361	.396	114.704	132
1.000	566.782	114.481	158.144	.261	.329	114.672	133

Fig. 10. The airfoil sections have considerable openness. One engineering procedure to close the gap is to rotate the lower surface about the leading edge. The inverse procedure in its present form needs a more rigorous trailing edge closure model. Two such candidate procedures are described in the next section as recommendations for further study.

RECOMMENDATIONS FOR FURTHER STUDY

Trailing Edge Closure

When a favorable pressure distribution is prescribed, it doesn's guarantee the resulting trailing edge thickness distribution to come out satisfactorily. To some extent, the trailing edge thickness can be controlled by adjusting the leading edge shape or the velocity potential value at the leading edge. Procedures to implement these ideas are described here.

Leading Edge (Nose) Shape Alteration

In a mixed analysis-inverse problem where the shape near the nose is usually prescribed and the objective is to weaken the shock or move the shock downstream, the shape of the nose can be used to control the trailing edge thickness. First, specify the nose shape given locally by $y = a_0 x^n$, where n and a_0 are two free parameters, and specify the desired C_p on the rest of

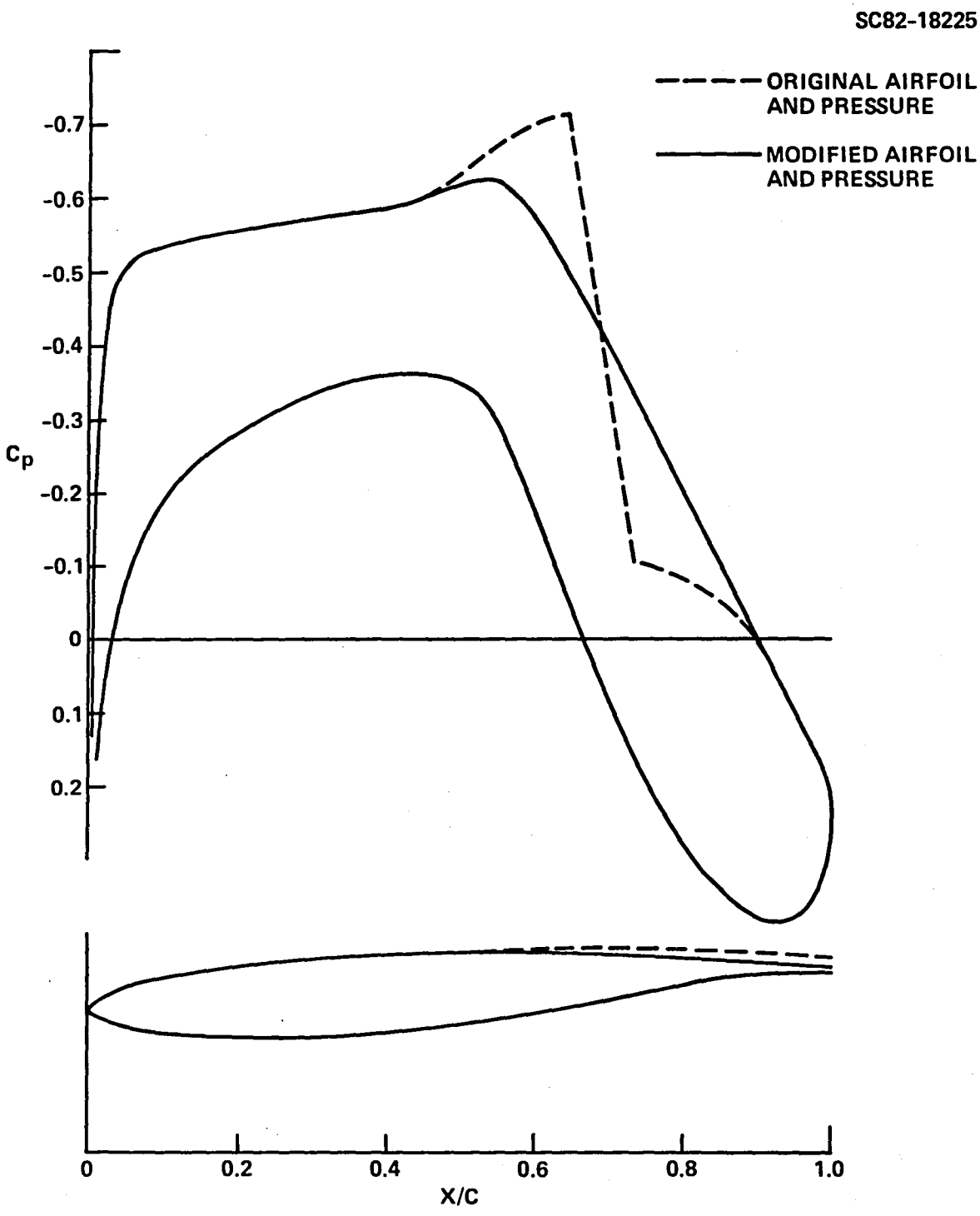

Fig. 6. Modified shape to weaken the shock system, $\eta = 0.6932$, $M_\infty = 0.86$, $\alpha = 4.86°$

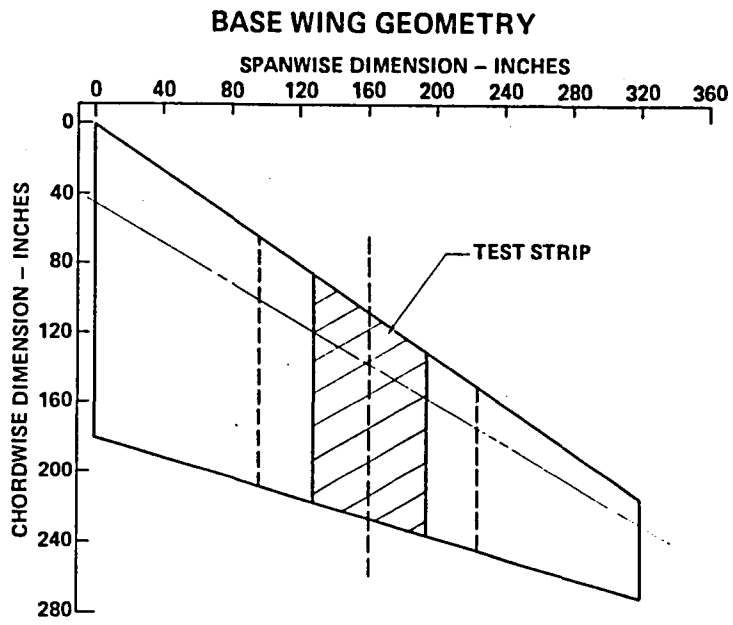

Fig. 7. Base wing geometry with a test strip where wing modification is required

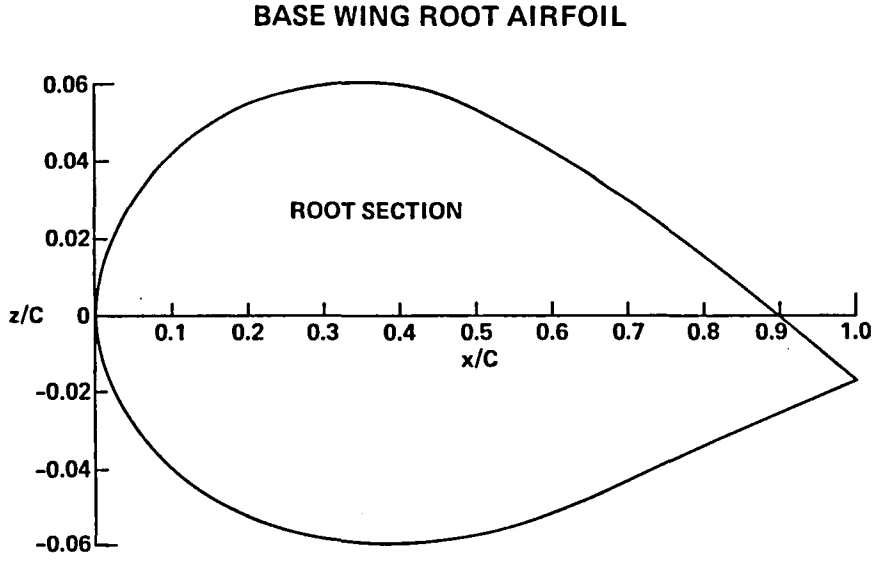

Fig. 8. Base wing airfoil geometry at the root section

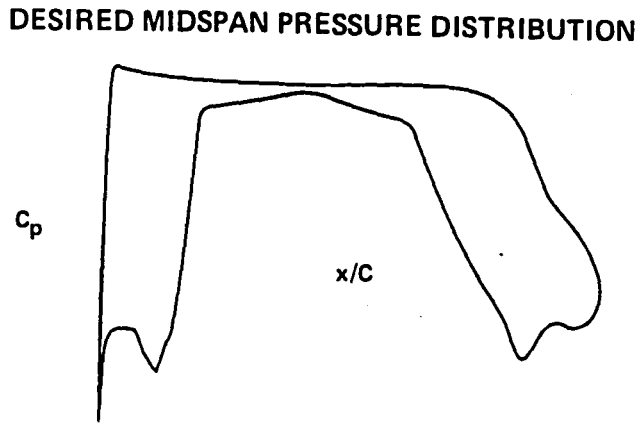

Fig. 9. Desired streamwise pressure distribution

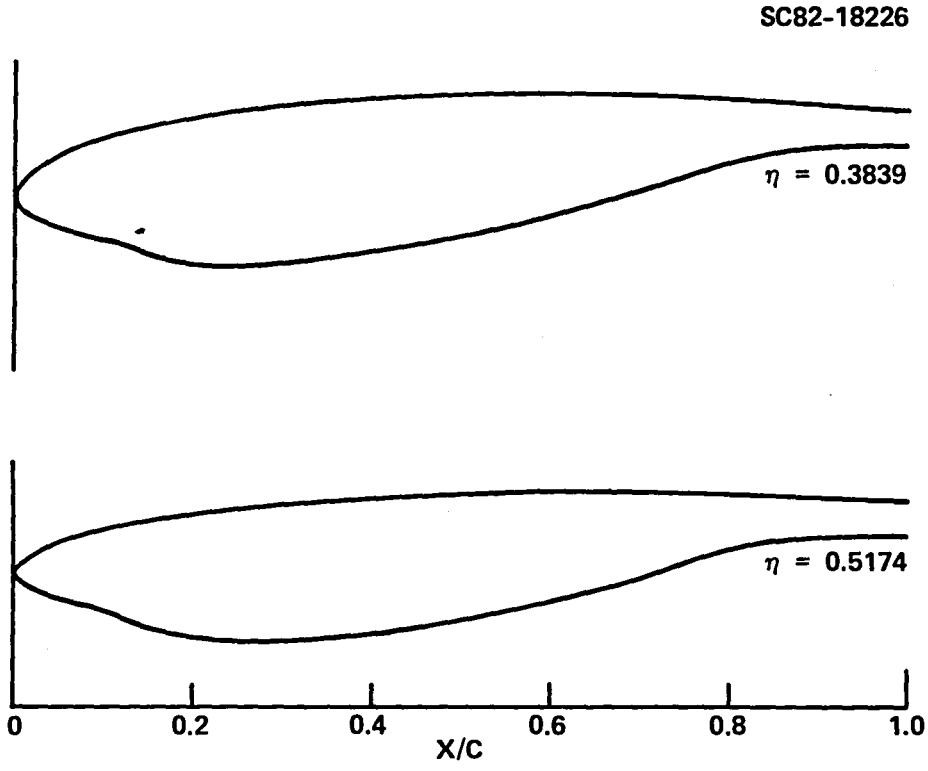

Fig. 10. Modified airfoil shapes at two different span stations to provide laminar flow control pressure distribution at midspan

the surface. The free parameters a_0 and n will then have to be adjusted using a gradient approach to satisfy a preset trailing edge thickness constraint. This method could possibly involve a mismatch in pressure at the point of transition from the analysis nose region to the C_p prescribed inverse region. If a mismatch in pressure occurs, then the specified pressure in the transition region must be allowed to vary to preserve a smooth pressure distribution.

Leading Edge Velocity Potential Alteration

In the case of a small disturbance methodology[4], the trailing edge closure was obtained by an alteration of the nose velocity potential. Such a procedure can also be tried in this full potential formulation. Let us define t_k to be the trailing edge thickness for the k^{th} span station. The objective then is to drive this t_k to some preset value (will be zero for closed trailing edge airfoil) by perturbing the velocity potential ϕ residing at the leading edge which is denoted by ϕ_{NOSE}. Denoting the functional relationship of t_k as $t_k = t_k(\phi_{NOSE})$, then one can write the following expansion

$$\left.\begin{aligned} t_k\left[\left(\phi_{NOSE} + \Delta\phi_{NOSE}\right)\right] = t_k\left(\phi_{NOSE}\right) + \left[\frac{\partial t_k}{\partial\left(\phi_{NOSE}\right)_m}\right]\Delta\left(\phi_{NOSE}\right)_m + \cdots \\ m = k_s, \cdots, k-1, k, k+1, \cdots, k_e \\ k = k_s, \cdots, k-1, k, k+1, \cdots, k_e \end{aligned}\right\} \quad (18)$$

where k_s and k_e denote the first inboard and final outboard span stations under design mode, respectively. For trailing edge closure condition, the left hand side of Eq. (18) is set to zero which yields enough equations to uniquely solve for all $\left(\Delta\phi_{NOSE}\right)_m$

$$\left\{\Delta\phi_{NOSE}\right\} = -\left[\frac{\partial t_k}{\partial\left(\phi_{NOSE}\right)_m}\right]^{-1}\left\{t_k\right\} \quad . \quad (19)$$

The $\{\Delta\phi_{NOSE}\}$ solution vector from Eq. (19) gives the amount of alteration to be made on $\{\phi_{NOSE}\}$ to drive $\{t_k\}$ to zero. In Eq. (19), the $\{\ \}$ symbol denotes a vector and $[\ ]^{-1}$ denotes the inverse of a matrix. Each element of this matrix is a partial derivative and a complete evaluation of all the matrix elements and the subsequent matrix inverse can be very costly and time-consuming, especially if several span stations are under design mode. To substantially reduce the computer time in the evaluation of matrix elements in Eq. (19), some tricks are used. First, the span station which has the maximum openness or fishtail is selected. For this span station (call it $k = k_t$) the influence function $\frac{\partial t_k}{\partial(\phi_{NOSE})_{k_t}}$ is generated and that influence function distribution is kept the same for all other design span stations but the magnitude is scaled by the following

$$\frac{\partial t_k}{\partial(\phi_{NOSE})_m} = \left(\frac{\partial t_k}{\partial(\phi_{NOSE})_{k_t}}\right) \frac{\frac{\Delta t_m}{\Delta(\phi_{NOSE})_m}}{\frac{\Delta t_{k_t}}{\Delta(\phi_{NOSE})_{k_t}}} \tag{20}$$

$$m = k_s, \cdots, k-1, k, k+1, \cdots, k_e \ .$$

It is recommended that both these procedures be tried in the currently developed inverse program. Besides the trailing edge closure model, further work is also recommended to assess the importance of pressure constraints in the inverse setting and the relationship between prescribed pressure and the freestream Mach number.

CONCLUSIONS

An inverse procedure based on the full potential equation in conservation form has been developed for use in recontouring a given wing to produce a prescribed favorable pressure distribution. A density linearization scheme is introduced to aid in the application of the pressure boundary condition. The inverse logic is incorporated into the existing finite volume FL030 analysis computer program. The new shape information is obtained from a mass flux integration procedure. The method is reasonably inexpensive and can be effectively used for shockless or shocked flow wing design. Two procedures to control the trailing edge are proposed for further study.

APPENDIX A

DERIVATION OF EQ. (11) IN THE DENSITY LINEARIZATION SECTION

For simplicity, the derivation shown here is for two dimensions and the extension to three dimensions is straightforward. Considering only the ζ,η directions, the contravariant velocities U and V can be written as

$$\left.\begin{aligned} U &= u\zeta_x + v\zeta_y = A_1\phi_\zeta + A_2\phi_\eta \\ V &= u\eta_x + v\eta_y = A_2\phi_\zeta + A_3\phi_\eta \end{aligned}\right\} \qquad \text{(A-1)}$$

where

$$A_1 = \zeta_x^2 + \zeta_y^2$$

$$A_2 = \zeta_x\eta_x + \zeta_y\eta_y$$

$$A_3 = \eta_x^2 + \eta_y^2$$

and u and v are the Cartesian velocity components along x and y. Using Eq. (A-1), the expression for density can be written as

$$\rho(\phi) = \left[1 - \frac{\gamma-1}{2} M_\infty^2(A_1\phi_\zeta^2 + 2A_2\phi_\zeta\phi_\eta + A_3\phi_\eta^2 - 1)\right]^{1/(\gamma-1)}. \qquad \text{(A-2)}$$

The change in density due to small changes in the velocity potential ϕ can be analyzed by substituting $(\phi + \delta\phi)$ for ϕ in Eq. (A-2).

$$\rho(\phi+\delta\phi) = \left[1 - \frac{\gamma-1}{2} M_\infty^2 \left\{A_1(\phi_\zeta+\delta\phi_\zeta)^2 + 2A_2(\phi_\zeta+\delta\phi_\zeta)(\phi_\eta+\delta\phi_\eta) + A_3(\phi_\eta+\delta\phi_\eta)^2 - 1\right\}\right]^{1/(\gamma-1)}$$

$$\doteq \left[1 - \frac{\gamma-1}{2} M_\infty^2 \left\{A_1\phi_\zeta^2 + 2A_2\phi_\zeta\phi_\eta + A_3\phi_\eta^2 + 2A_1\phi_\zeta\delta\phi_\zeta + 2A_2(\phi_\zeta\delta\phi_\eta + \phi_\eta\delta\phi_\zeta) + 2A_3\phi_\eta\delta\phi_\eta - 1\right\}\right]^{1/(\gamma-1)}$$

$$= \rho(\phi)\left\{1 - \frac{(\gamma-1)M_\infty^2}{[\rho(\phi)]^{\gamma-1}}\left[A_1\phi_\zeta\delta\phi_\zeta + A_2(\phi_\zeta\delta\phi_\eta + \phi_\eta\delta\phi_\zeta) + A_3\phi_\eta\delta\phi_\eta\right]\right\}^{1/(\gamma-1)}$$

$$\rho(\phi+\delta\phi) \doteq \rho(\phi)\left\{1 - \frac{M_\infty^2}{[\rho(\phi)]^{\gamma-1}}\left[U\delta\phi_\zeta + V\delta\phi_\eta\right]\right\} \qquad \text{(A-3)}$$

$$\delta\rho = \rho(\phi+\delta\phi) - \rho(\phi) = -\rho^{2-\gamma}M_\infty^2\left[U\delta\phi_\zeta + V\delta\phi_\eta\right]$$

$$= -\rho^{2-\gamma}M_\infty^2\left[U\frac{\partial}{\partial\zeta} + V\frac{\partial}{\partial\eta}\right]\delta\phi \qquad \text{(A-4)}$$

differential operator $\left(\frac{\partial\rho}{\partial\phi}\right)$

Equation (A-4) is the two dimensional analog of Eq. (11) in the main report.

APPENDIX B

INSTRUCTIONS FOR THE USE OF THE INVERSE CODE IN ITS PRESENT FORM

1. In subroutine XSWEEP (after XSWEEP.15), the user specifies the following information.

   a. IDU ∿ I index of the first upper surface point from the leading edge where inverse calculation starts.

   b. IDL ∿ I index of the first lower surface point where inverse calculation starts.

   c. KNIB ∿ First inboard span station index K where inverse calculation starts.

   d. KOUTB ∿ Last outboard span station where inverse calculation ends.

2. Specification of modified pressures at half node points under the dimensional array name CPD(I,K), in the main program after MAIN.80.

3. The format of the output is shown in Tables 1 and 2 and explanations of columns (1) to (8) are given on pages 12 and 13.

REFERENCES

1. Murman, E.M. and Cole, J.D., "Calculation of Plane Steady Transonic Flow," AIAA Journal, Vol. 9, No. 1, January 1971, pp. 114-121.
2. Shankar, V., Malmuth, N.D., and Cole, J.D., "Computational Transonic Airfoil Design in Free Air and a Wind Tunnel," AIAA Paper No. 78-103, January 1978.
3. Shankar, V., Malmuth, N.D., and Cole, J.D., "Computational Transonic Design Procedure for Three Dimensional Wings and Wing-Body Combinations," AIAA Paper No. 79-0344, 1979.
4. Shankar, V., "Computational Transonic Inverse Procedure for Wing Design with Automatic Trailing Edge Closure," AIAA Paper No. 80-1390, July 1980.
5. Tranen, T.L., "A Rapid Computer Aided Transonic Airfoil Design Method," AIAA Paper No. 74-501, June 1974.
6. Carlson, L.A., "Transonic Airfoil Analysis and Design Using Cartesian Coordinates," Proc. AIAA 2nd Computational Fluid Dynamics Conference, June 19-20, 1975, pp. 175-183.
7. Henne, P.A., "Inverse Transonic Wing Design Method," Journal of Aircraft, Vol. 18, No. 2, February 1981.
8. Jameson, A., "Iterative Solution of Transonic Flows over Airfoils and Wings Including Flows at Mach 1," Comm. Pure and Appl. Math., Vol. 27, pp. 283-309, 1974.
9. Lax, P.D., "Weak Solutions of Nonlinear Hyperbolic Equations and Their Numerical Computation," Comm. Pure and Appl. Math., Vol. 7, No. 1, 1954, pp. 159-193.
10. Sobieczky, H., Yu, N.J., Fung, K.Y., and Seebass, A.R., "A New Method for Designing Shock-Free Transonic Configurations," AIAA Paper No. 78-1114, 1978.
11. Fung, H.Y., Sobieczky, H., and Seebass, R., "Numerical Aspects of the Design of Shock-Free Wings and Wing-Body Combinations," AIAA Paper No. 79-1557, 1979.
12. Yu, N.J., "An Efficient Transonic Shock-Free Wing Redesign Procedure Using a Fictitious Gas Method," AIAA Paper No. 79-0075, 1979.
13. Hicks, R.M. and Henne, P.A., "Wing Design by Numerical Optimization," AIAA Paper No. 77-1247, 1977.
14. Holst, T.L., "A Fast, Conservative Algorithm for Solving the Transonic-Potential Equation," AIAA Paper No. 79-1456, July 1979.
15. Jameson, A. and Caughey, D.A., "A Finite Volume Method for Transonic Potential Flow Calculations," AIAA Paper No. 77-635, June 1977.
16. Caughey, D.A. and Jameson, A., "Numerical Calculation of Transonic Potential Flow about Wing-Body Combinations," AIAA Journal, Vol. 17, No. 2, February 1979.

1. Report No.	2. Government Accession No.	3. Recipient's Catalog No.
NASA CR-165991		

4. Title and Subtitle	5. Report Date
A FULL POTENTIAL INVERSE METHOD BASED ON A DENSITY LINEARIZATION SCHEME FOR WING DESIGN	October 1982
	6. Performing Organization Code
7. Author(s)	8. Performing Organization Report No.
Vijaya Shankar	SC5277.21FR
	10. Work Unit No.
9. Performing Organization Name and Address	
Rockwell International Science Center P.O. Box 1085 Thousand Oaks, California 91360	11. Contract or Grant No. NAS1-16379
	13. Type of Report and Period Covered Contractor Report 08/29/80 thru 08/28/81
12. Sponsoring Agency Name and Address	14. Sponsoring Agency Code
National Aeronautics and Space Administration Washington, D.C. 20546	

15. Supplementary Notes

Langley Technical Monitor: James D. Keller
Final Report

16. Abstract

A mixed analysis-inverse procedure based on the full potential equation in conservation form has been developed to recontour a given base wing to produce a prescribed favorable pressure distribution. The method incorporates a novel density linearization scheme in applying the pressure boundary condition in terms of the velocity potential. The FL030 finite volume analysis code has been modified to include the inverse option. The new surface shape information, associated with the modified pressure boundary condition, is calculated at a constant span station based on a mass flux integration. The inverse method is shown to recover the original shape when the analysis pressure is not altered. Inverse calculations for weakening of a strong shock system and for a laminar flow control (LFC) pressure distribution are presented. Two methods for a trailing edge closure model are proposed for further study.

17. Key Words (Suggested by Author(s))	18. Distribution Statement
Full potential formulation Inverse problem Density linearization Wing design Transonic flow	Unclassified - unlimited Subject Category 02

19. Security Classif. (of this report)	20. Security Classif. (of this page)	21. No. of Pages	22. Price
Unclassified	Unclassified	30	

N-305

For sale by the National Technical Information Service, Springfield, Virginia 22161

End of Document